RSC Advances

ROYAL SOCIETY OF CHEMISTRY

www.rsc.org/advances

Graphical Abstract

Co_xP compounds: Electrochemical conversion/partial recombination reaction and partially disproportionated nanocomposite for Li-ion battery anodes

Hyuk-Tae Kwon, Jae-Hun Kim, Ki-Joon Jeon and Cheol-Min Park*

In this report, Co_xP binary compounds and their nanocomposites were synthesized using simple solid-state synthetic routes, and their potential as anode materials for Li-ion batteries was investigated.

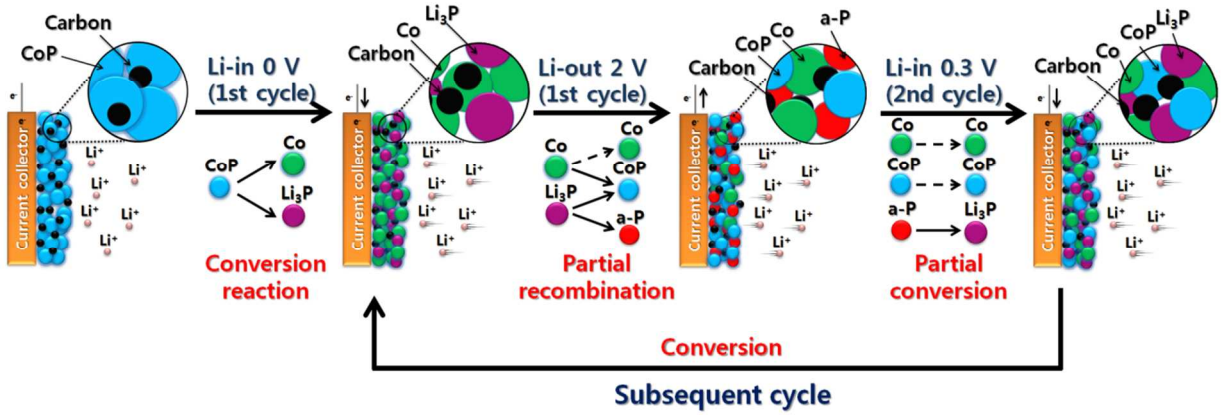

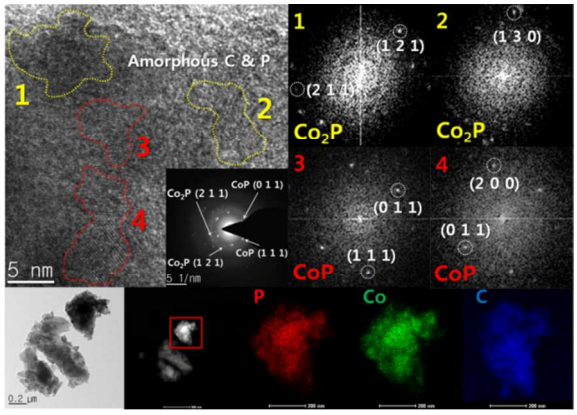

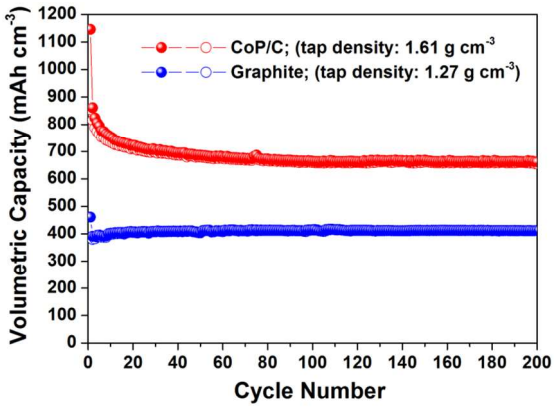

RSC Advances

RSCPublishing

ARTICLE

Co_xP compounds: Electrochemical conversion/partial recombination reaction and partially disproportionated nanocomposite for Li-ion battery anodes

Cite this: DOI: 10.1039/x0xx00000x

Received 00th July 2014,
Accepted 00th July 2014

DOI: 10.1039/x0xx00000x

www.rsc.org/

Hyuk-Tae Kwon[a], Jae-Hun Kim[b], Ki-Joon Jeon[c] and Cheol-Min Park*[ad]

Co_xP binary compounds, CoP and Co_2P, were synthesized using simple solid-state synthetic routes, and their potential as anode materials for Li-ion batteries was investigated. Electrochemical Li reactivity was possible on the CoP electrode, whereas the Co_2P electrode did not react with Li. The electrochemically driven partial recombination reaction of the CoP electrode was thoroughly demonstrated using ex situ X-ray diffraction and extended X-ray absorption fine structure analyses. To enhance the electrochemical performances of CoP, its carbon-modified nanocomposite was prepared. The nanocomposite consisted of well-dispersed CoP (active with Li) and Co_2P (inactive with Li) nanocrystallites, as well as amorphous P within the amorphous carbon matrix. The partially disproportionated CoP/C nanocomposite electrode exhibited good electrochemical performance with a high initial charge capacity of 531 mA h g^{-1} (or 855 mA h cm^{-3}), a cycling durability of 407 mA h g^{-1} (or 655 mA h cm^{-3}) over 200 cycles, a good initial coulombic efficiency of ca. 75%, and a fast rate capability (2C: 435 mA h g^{-1}, 3C: 410 mA h g^{-1}).

Introduction

As fossil fuels are being exhausted, the development of long-lasting energy storage systems is needed to satisfy the need for electronic mobile devices and hybrid electric vehicles (HEVs). Among the various energy storage systems, the Li-ion battery is considered a promising choice because of its large energy density, fast rate capability, and high power. Graphite is widely used at present as an anode material in rechargeable Li-ion battery systems because Li intercalates into the gaps in the graphene layer. However, the demand is constantly increasing for advanced battery materials with higher gravimetric and volumetric energy densities than the graphite anode because the graphite anode has a limited theoretical capacity corresponding to the formation of LiC_6 (372 mA h g^{-1} or ca. 840 mA h cm^{-3}).[1-10] Among the many possible alternatives, Li alloy-based systems, such as Sn-based oxides,[11-15] Si-based composites,[16-20] transition metal oxides,[21-24] metal phosphides,[25-39] and metal antimonide systems,[40-44] have been focused on owing to their ability to react reversibly with large amounts of Li per formula unit. Although Li alloy-based systems have a higher energy density, they suffer from poor capacity retention because of large volume changes that occur during charge/discharge.

Transition metal phosphides, M_xP_y (M = Ti, V, Mn, Fe, Co, Ni, Cu, or Zn; x = 1 or 2; y = 1, 2, 3, or 4), are a very attractive negative electrode material for Li secondary batteries because they have high specific capacities that depend on the phosphorus content (Li_3P: 2596 mA h g^{-1}) and an interesting reaction mechanism.[26-39] Li can form two different types of complexes with the transition metal phosphides: (i) Li ternary phase through an insertion (or addition) reaction and (ii) Li_3P phase with a nanocrystalline metal by a conversion reaction. The insertion and conversion reactions can be summarized as follows:

Insertion (addition) reaction: $M_xP_y + zLi \rightarrow Li_zM_xP_y$ (1)
Conversion reaction: $M_xP_y + 3Li \rightarrow yLi_3P + xM$ (2)

The formation of $Li_zM_xP_y$ by insertion reaction (1) results in good electrochemical behavior attributable to stable crystalline structures, which is advantageous for high-performance anode materials. Souza et al. demonstrated a quasi-topotactic-intercalation mechanism, where lithium is inserted into the binary MnP_4 phase to form a cubic ternary Li_7MnP_4 phase.[26] Furthermore, a quasi-intercalation reaction between black phosphorus and a LiP phase,[25] as well as a topotactic reaction between VP and a LiVP phase,[27] were reported by Park et al. On the other hand, conversion reaction (2) produces a

nanocrystalline metal and Li_3P, which affords advantageous features in terms of less severe structural stress. Most P-based compounds show the conversion reaction when the electrodes were fully Li inserted phase.[26-39]

The interesting insertion/extraction behaviors of P-based materials have motivated numerous studies into the use of these materials as possible Li-ion battery anodes. Among the various P-based materials, Co-P binary compounds (CoP_3, CoP, and Co_2P) have been actively investigated by many researchers. Co-P compounds can be synthesized easily using solid-state synthetic routes, such as heat-treatment and the ball-milling technique, and have high reversible capacities of >1000 mA h g^{-1}. Owing to these favorable properties, various materials using Co-P compounds have been reported, including pulsed laser deposited CoP thin films, partially lithiated CoP_x, electrodeposited Co-P alloys, and thermally decomposed Co_xP nanostructures. However, the cycle performances of these materials are still poor.[33-39]

Based on the Co-P binary phase diagram, CoP and Co_2P compounds were synthesized using simple high energy mechanical milling (HEMM) and their suitability as anode materials for rechargeable Li-ion batteries was tested. The electrochemical reaction mechanism of the as-prepared CoP electrode is discussed in this paper on the basis of the ex situ X-ray diffraction (XRD) and extended X-ray absorption fine structure (EXAFS) analyses, along with the differential capacity plot (DCP). Additionally, to enhance the electrochemical performances of CoP, its carbon-modified nanocomposite was suggested as a high-performance anode material for rechargeable Li-ion batteries.

Experimental

Preparation of Nanocomposite: CoP and Co_2P were synthesized using the following solid-state synthetic route. Stoichiometric amounts of Co (Aldrich, 99.9%, average size: ca. 150 μm) and P (Kojundo, average size: ca. 75 μm) powders were placed in a hardened steel vial with a capacity of 80 cm^3 along with stainless steel balls (diameters: 3/8 in. and 3/16 in.) at a ball-to-powder weight ratio of 20:1. The vial was assembled in an argon-filled glove box and an HEMM process (Spex-8000) was conducted under an Ar atmosphere for 6 h. To obtain the CoP/C composite, the same HEMM process was carried out using the synthesized CoP powder and carbon (Super P, Timcal) for 6 h. The preliminary electrochemical tests showed that the optimal amounts of CoP and C were 60% and 40% by weight, respectively.

Materials Characterization: CoP and its composite samples were characterized using XRD (DMAX2500-PC, Rigaku), high-resolution transmission electron microscopy (HRTEM, FEI F20, operating at 200 kV), and energy-dispersive spectroscopy (EDS) coupled with HRTEM. Ex situ XRD and EXAFS analyses were used to observe the structural changes occurring in the active material of the CoP electrode during Li insertion/extraction. The Co K-edge EXAFS spectra for the CoP electrode were recorded at the 8C (Nano XAFS) beamline in a storage ring of 3.0 GeV at the Pohang Light Source (PLS), South Korea.

Electrochemical Measurements: For the electrochemical evaluation of Co_2P, CoP, and its composite, the electrodes were prepared by coating a copper foil substrate with a slurry consisting of the active powder material (70 wt%), carbon black (Denka, 15 wt%) as a conducting agent, and polyvinylidene fluoride (PVdF, 15 wt%) dissolved in *N*-methyl-2-pyrrolidone (NMP) as a binder. Samples of each mixture were vacuum-dried at 120 °C for 3 h and pressed. The electrodes were composed of ca. 0.05 mm thickness and 0.79 cm^2 area with ca. 2.3 mg weight of CoP/C composite (with ca. 1.9 mg weight of graphite). Coin-type electrochemical cells were assembled in an Ar-filled glove box using Celgard 2400 as the separator, Li foil as the counter and reference electrodes, and 1 M $LiPF_6$ in ethylene carbonate/diethyl carbonate (EC/DEC, 1:1 by volume, Panax STARLYTE) as the electrolyte. All the cells were tested galvanostatically between 0.0 and 2.0 V (vs. Li/Li^+) at a current density of 100 mA g^{-1} using a Maccor automated tester, with the exception of the rate-capability tests. The gravimetric capacity was calculated on the basis of the weight of the active materials, and the volumetric capacity was calculated by multiplying the gravimetric capacity by the tap density (CoP/C: 1.61 g cm^{-3}, graphite: 1.27 g cm^{-3}), which was measured using a powder tap density tester (BT-301, Bettersize). Li was inserted into the electrode during the discharge reaction and was extracted from the working electrode during the charge reaction.

Results and discussion

Figure 1a shows the binary Co-P phase diagram, which composed of two compounds, CoP and Co_2P.[45] Figures 1b and c show the XRD patterns of CoP and Co_2P, respectively, which were synthesized using a simple HEMM technique. The XRD patterns in Figures 1b and c corresponded to the CoP and Co_2P phases, respectively, and no other crystalline phases were detected. The crystalline structures of orthorhombic CoP (S.G. Pnma, a = 5.077 Å, b = 3.281 Å, c = 5.587 Å) and Co_2P (S.G Pnma, a = 5.646 Å, b = 6.609 Å, c = 3.513 Å) are shown in the insets of Figures 1b and c, respectively. The crystalline structure of CoP had more voids and channels for facile Li diffusion and storage than that of Co_2P, which indicated that CoP has significant potential for use as an anode material in rechargeable Li-ion batteries.

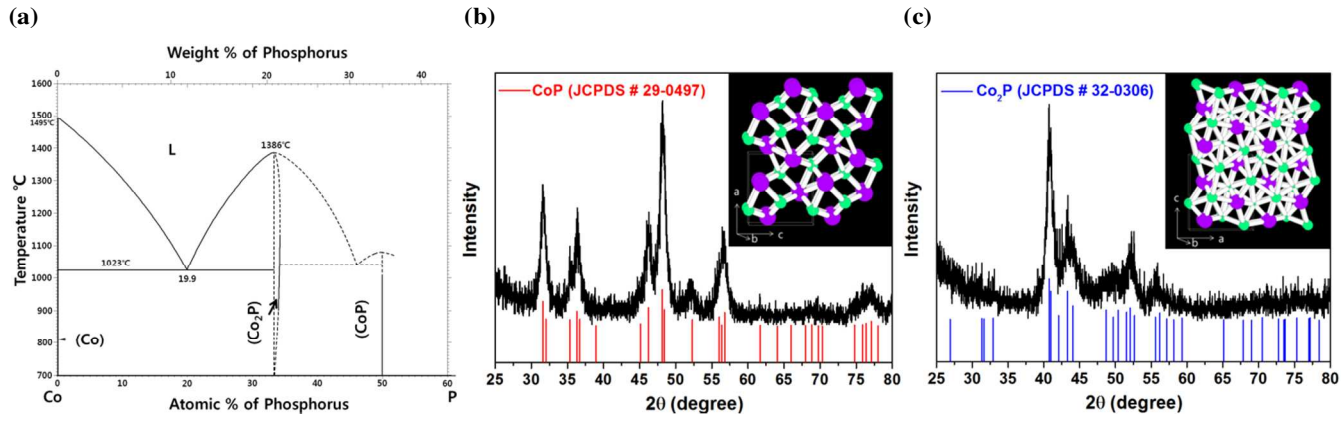

Figure 1 (a) Co-P binary phase diagram, and XRD patterns with ball-and-stick models (P: purple, Co: green) of the crystalline structures of (b) CoP and (c) Co_2P.

The voltage profiles of the CoP and Co_2P electrodes are shown in Figures 2a and b, respectively. The first discharge and charge capacities of the CoP electrode were 915 and 778 mA h g^{-1}, respectively, with a high initial coulombic efficiency of 85%. Considering the theoretical capacity of CoP (894 mA h g^{-1}) and a solid electrolyte interphase (SEI) layer formation reaction near 0.7 V, it can be concluded that the synthesized CoP electrode was fully reacted with Li. Although the CoP electrode exhibited a high initial coulombic efficiency, it showed poor cyclability. The drastic decrease in the capacity of the CoP electrode was caused by the large volume change due to the formation of Li_3P, which was associated with the pulverization of the active material as well as its electrical

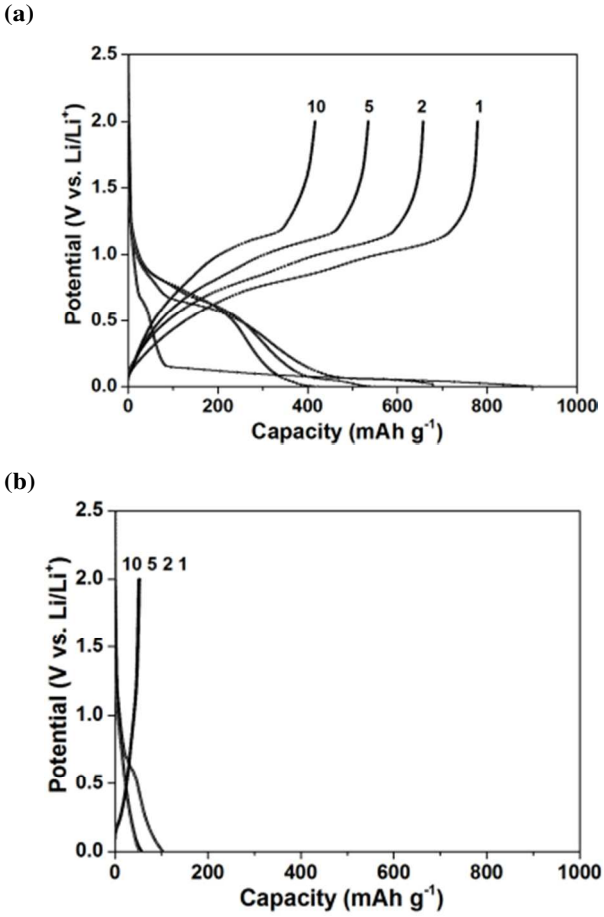

Figure 2 Voltage profiles of the (a) CoP and (b) Co_2P electrodes for the 1st, 2nd, 5th, and 10th cycles.

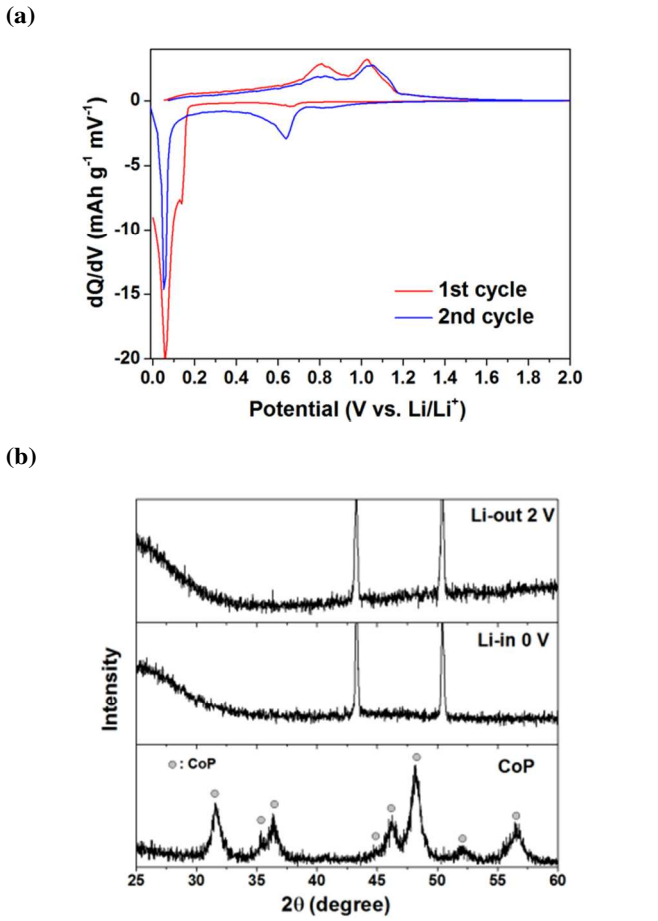

Figure 3 Electrochemical reaction mechanism between CoP and Li: (a) DCP of 1st and 2nd cycles and (b) ex situ XRD results for the 1st cycle.

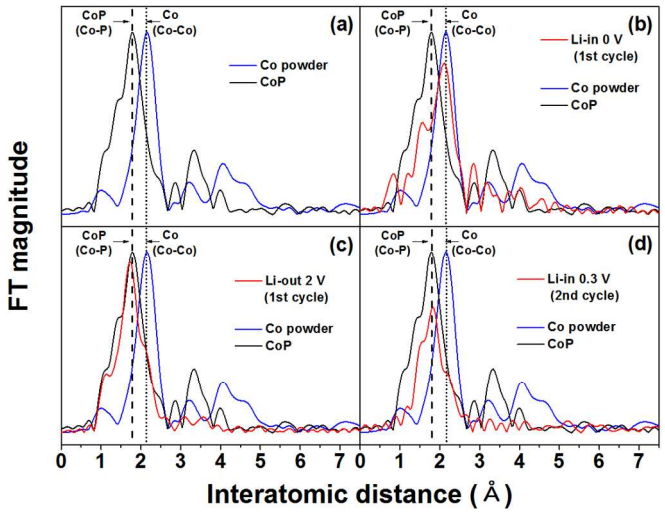

Figure 4 EXAFS spectra of the CoP electrode: (a) pristine CoP electrode, (b) Li insertion at 0 V (1st cycle), (c) Li extraction at 2 V (1st cycle), and (d) Li insertion at 0.3 V (2nd cycle).

isolation from the current collector. Considering the theoretical capacity (894 mA h g^{-1}) of the CoP electrode and the solid electrolyte interphase reaction of ca. 0.7 V, it can be concluded that the synthesized CoP electrode was fully reacted with Li. On the other hand, small discharge and charge capacities were observed for the Co_2P electrode owing to the reaction of the carbon conducting agent, which indicated that Co_2P was inactive with Li. The inactivity of Co_2P toward Li may be related to the high overpotential that caused the break up the Co–P bonds as above mentioned in comparison with the crystalline structure.

The DCP for the first cycle of the CoP electrode (Figure 3a) showed a large peak at 0.05 V during the discharge reaction and two broad peaks at 0.8 and 1.0 V during the charge reaction. In the second cycle, two DCP peaks at 0.64 and 0.05 V were observed during the charge reaction, whereas the DCP peaks during the discharge reaction were the same as those of the first cycle, indicating the involvement of interesting electrochemical reactions. Ex-situ XRD analyses (Figure 3b) were performed at the fully discharged state (0 V) and the fully charged state (2.0 V). However, no structural changes due to the amorphization of the active materials were observed for the CoP electrode during the discharge and charge reactions.

To confirm the electrochemical reaction mechanism of the CoP electrode with more detail, Co K-edge EXAFS analyses of the CoP electrode were performed at selected potentials as referenced in the DCP (Figure 3a), and the results are shown in Figure 4. Figure 4a shows that the main EXAFS peaks in the spectrum for the crystalline CoP and metallic Co were associated with the Co–P interatomic bond length (1.78 Å) and Co–Co interatomic bond length (2.14 Å), respectively. When the electrode was fully discharged to 0 V for the first cycle (Figure 4b), the main EXAFS peak of the CoP phase was that of the Co metal showing the spectrum associated with the Co–Co interatomic bond length (2.14 Å). In the fully charged state of 2.0 V (Figure 4c), the two main EXAFS peaks, corresponding to the Co (2.14 Å) and CoP (1.78 Å) phases, appeared together, which demonstrated that the CoP phase was partially recombined during the charge reaction of the first cycle. To confirm the DCP peak at 0.65 V during the second discharge, which was not observed in the first cycle (Figure 3a), EXAFS analysis at the potential of 0.3 V during the second discharge was analyzed as shown in Figure 4d, which showed no variation. This result indicated that the remaining P resulted from the partial recombination reaction was reacted with Li. The potential at ca. 0.65 V coincided with the reaction potential for the reaction between P and Li (P → Li_3P),[25] which also indicated the partial recombination reaction of the CoP electrode during the charge reaction. On the basis of the above DCP and EXAFS results, the reaction mechanisms of the first and subsequent cycles are suggested as follows:

During the first cycle of the CoP electrode:
- Discharge: CoP → Li_3P + Co
- Charge: Li_3P + Co → CoP + Co + P

Subsequent cycles of the CoP electrode:
- Subsequent discharge/charge: CoP + Co + P ⇄ Li_3P + Co

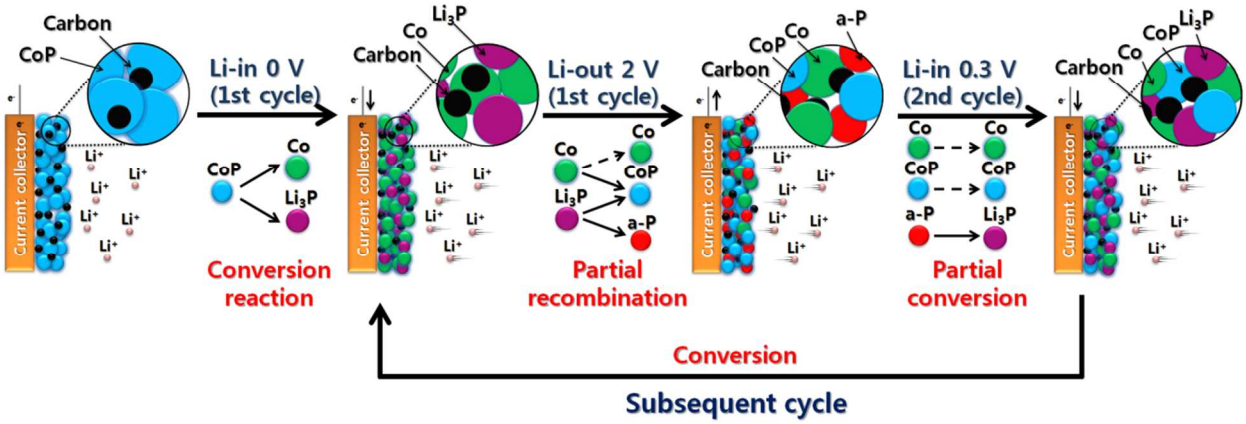

Figure 5 Schematic diagram of the electrochemical reaction mechanism of the CoP electrode during cycling.

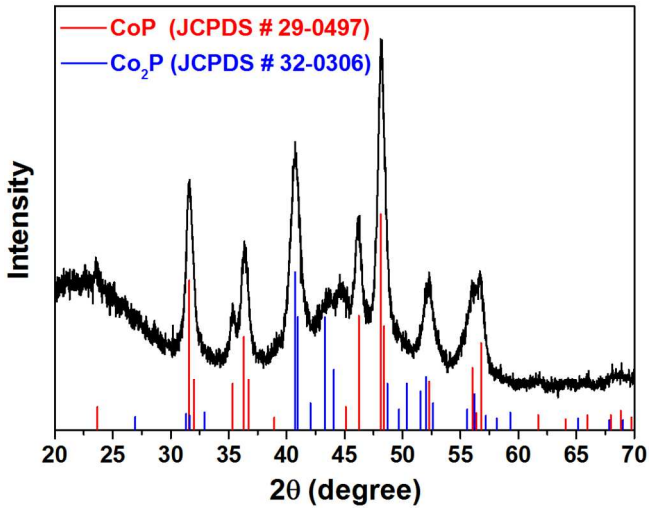

Figure 6 XRD pattern of the CoP/C nanocomposite.

Figure 5 shows a schematic diagram for the electrochemical conversion and partial recombination reaction of the CoP electrode during cycling. The EXAFS spectra clearly demonstrated the partial recombination of the CoP electrode during charge, which is a distinctive behavior for this electrode when compared with the reaction mechanisms of previously studied electrodes consisting of Co-P compounds.[33-39] Generally, the recombination reaction during charge is advantageous in terms of the electrochemical performance of Li alloy-based anodes. This is because the compound phase is gradually decreased to nanocrystallites of 2–3 nm after a few cycles, which retain the same size throughout subsequent discharge/charge cycles by repeated conversion and recombination to form the compound phases within the composite.[44,46-48]

Nanostructured composite materials are considered to be promising alternative solutions for high performance anode materials because they offer the following advantages: high capacity owing to their ability to provide a higher interfacial area, high rate capability because of their increased lithium ion diffusion rate, and stable cycling behavior owing to their ability to accommodate the strain generated during cycling.[6,42,46,49] Among the various synthetic methods available for nanostructured composite materials, HEMM was most suitable for fabricating high-performance electrode materials. The HEMM technique plastically deforms the particles, which leads to work hardening and fracture of materials upon impact at temperature >200 °C and pressures on the order of 6 GPa.[50] Upon consideration of the HEMM mechanism, the CoP/C nanocomposite was prepared using HEMM. In the XRD pattern of the CoP/C nanocomposites (Figure 6), two phases composed of Co_2P and CoP were confirmed, which indicated that the CoP phase within the CoP/C composite was partially disproportionated to Co_2P and P (amorphous) as a result of the HEMM process. A similar disproportionation reaction has also been observed for SiO and $CoSb_x$ samples.[51,52] SiO was disproportionated to nanocrystalline Si and SiO_2 at high temperatures.[51] $CoSb_3$ and $CoSb_2$ were disproportionated to nanocrystalline $CoSb_2$ + Sb (amorphous) and CoSb + Sb (amorphous), respectively, by HEMM.[52] The composition ratio of CoP, Co_2P, amorphous P, and carbon in the partially disproportionated CoP/C composite was calculated using the Jade 9 software to compare the XRD peak intensities and was approximately 30:25:5:40 by weight, respectively.

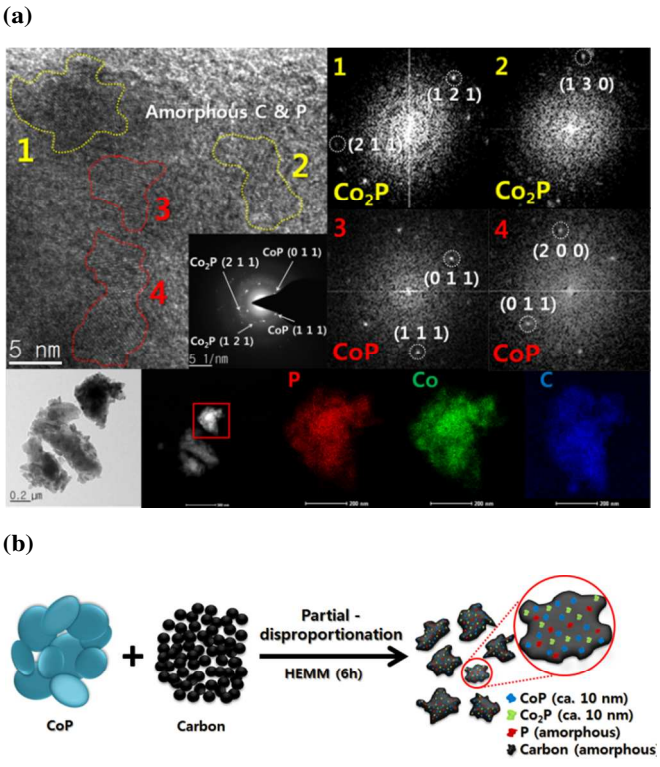

Figure 7 (a) TEM bright-field, HRTEM image combined with selected area diffraction pattern and FT patterns, STEM and its EDS mapping images, and (b) Schematic view of the disproportionated CoP/C nanocomposite.

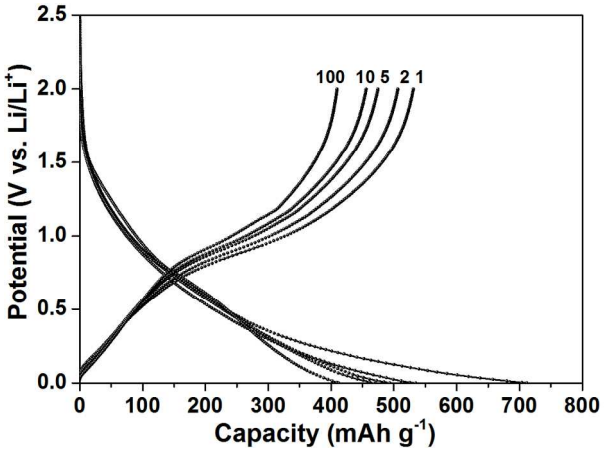

Figure 8 Voltage profile of the CoP/C nanocomposite electrode for the 1st, 2nd, 5th, 10th, and 100th cycles.

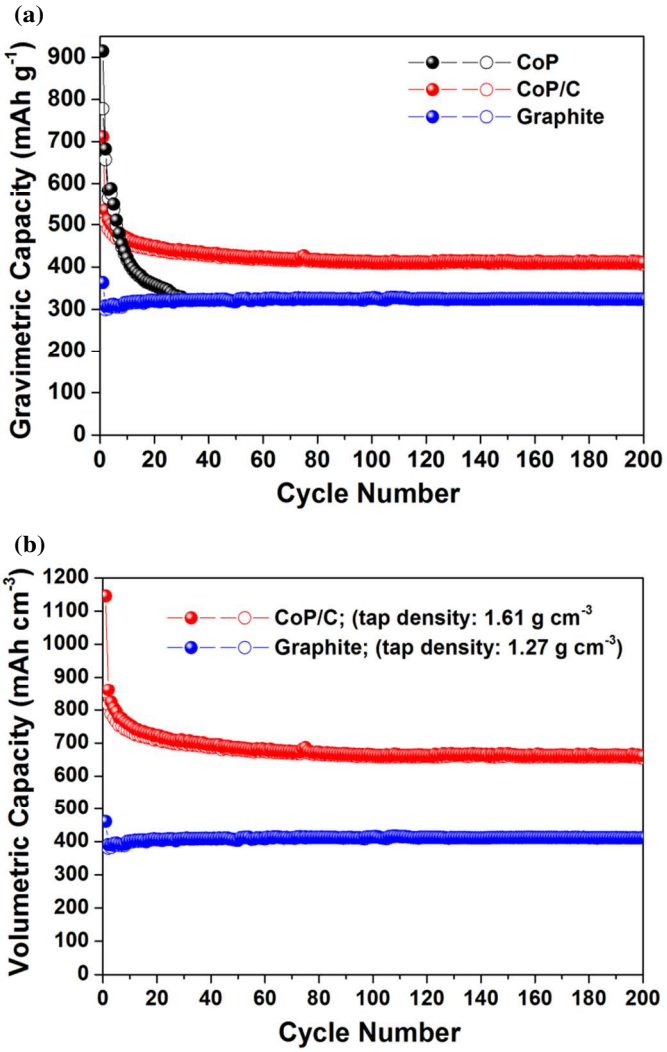

Figure 9 Comparison of the cycle performance of the graphite (MCMB), CoP, and disproportionated CoP/C nanocomposite electrodes at a cycling rate of 100 mA g^{-1}: (a) gravimetric capacity vs. cycle numbers and (b) volumetric capacity vs. cycle numbers.

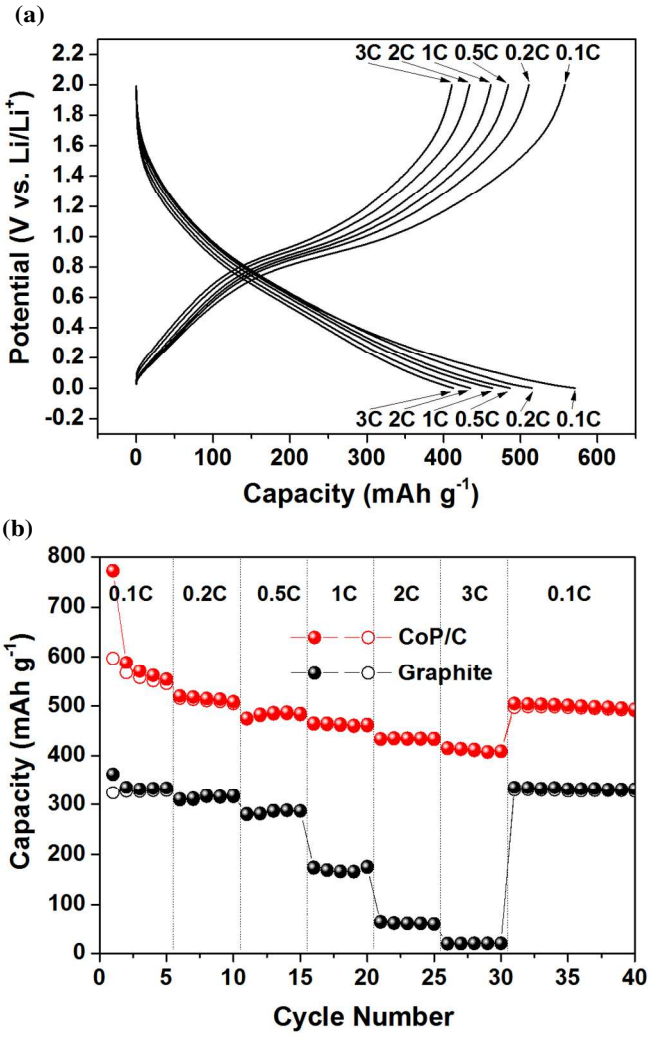

Figure 10 Comparison of the rate capability: (a) voltage profile at various C rates for the CoP/C nanocomposite electrode and (b) plot of the discharge and charge capacity vs. cycle number for the CoP/C nanocomposite and graphite (MCMB) electrodes at various C rates. (CoP/C: 1C – 530 mA g^{-1}, graphite: 1C – 320 mA g^{-1})

The TEM bright-field and HRTEM images combined with selected-area diffraction (SAD) patterns and lattice spacing of the CoP/C nanocomposite are shown in Figure 7a. The SAD patterns showed both CoP and Co_2P phases, which indicated that some CoP within the CoP/C composite was partially disproportionated to ca. 10 nm-sized nanocrystalline Co_2P and amorphous P, which is in agreement with the XRD results. The EDS mapping image confirmed that the nanocrystalline CoP and Co_2P, amorphous P, and amorphous carbon were well dispersed within the composite, as shown in Figure 7a. Therefore, it can be concluded that the CoP/C nanocomposite was composed of CoP (ca. 10 nm), partially disproportionated Co_2P (ca. 10 nm), amorphous P, and amorphous carbon as illustrated schematically in Figure 7b.

The voltage profile of the CoP/C nanocomposite electrode is shown in Figure 8. The discharge and charge capacities of the first cycle for the CoP/C nanocomposite electrode within the voltage range of 0–2.0 V were 712 and 531 mA h g^{-1} (or 1146 and 855 mA h cm^{-3}), respectively, with a relatively high initial coulombic efficiency of 75%. The initial irreversible capacity owing to the ball-milled amorphous carbon content (40 wt%) of the CoP/C nanocomposite was approximately 180 mA h g^{-1}, which demonstrates that the active materials, such as CoP and partially disproportionated amorphous P, in the composite electrode were fully reversible with Li. The good electrochemical Li reactivity with the CoP/C composite is attributed to the well-dispersed CoP (active with Li), nanocrystalline Co_2P (inactive with Li), and amorphous P (active with Li) within the amorphous carbon matrix formed by the partial disproportionation reaction.

Comparisons of the cycling performances were made for CoP, CoP/C, and the commercially available mesocarbon microbeads (MCMB)-graphite electrode cycled at 100 mA g^{-1} (voltage range: 0.0–2.0 V). The gravimetric and volumetric capacities of the CoP electrode, as shown in Figures 9a and b, respectively, decreased gradually after a few cycles. The capacity decrease was caused by mechanical cracking and crumbling, which was attributed to the large volume change during the formation of the Li_3P phase. The reversible capacity and capacity retention of the CoP/C nanocomposite electrodes were significantly enhanced compared with those of the CoP electrode. The CoP/C nanocomposite electrode showed a very stable capacity of 407 mA h g^{-1} (or 655 mA h cm^{-3}) for over 200 cycles, corresponding to ca. 77% of the initial charge capacity. The volumetric capacity of the CoP/C nanocomposite electrode was much higher than the MCMB-graphite electrode, as shown in Figure 9b. The good cycling behavior of the CoP/C nanocomposite electrode was attributed to the uniform distribution of active CoP nanocrystallites, the presence of a well-dispersed nanocrystalline Co_2P inactive matrix that prevents the agglomeration of active materials during cycling, and the amorphous carbon buffering matrix that alleviates the effect of the volume expansion on the active materials, as illustrated in Figure 7c.

The rate capability test of the CoP/C nanocomposite electrode was also conducted in the potential range between 0.0 and 2.0 V. Figures 10a and b show the cyclability of the CoP/C nanocomposite electrode as a function of the C rate, where C is defined as the full use of the restricted charge capacity of 530 mA h g^{-1} in 1 h. At rates of 2C and 3C, the CoP/C nanocomposite electrode showed very high charge capacities of 435 and 410 mA h g^{-1}, respectively, corresponding to ca. 79% and 75% of the charge capacity for the rate at 0.1C with stable cycling behavior. The rate capability of the CoP/C nanocomposite electrode was excellent compared with that of the commercially available MCMB-graphite electrode. The fast rate capability of the CoP/C nanocomposite electrode was ascribed to the presence of the ca. 10 nm-sized nanocrystalline CoP and partially disproportionated amorphous P, which contributed short Li diffusion paths. Additionally, the well-dispersed, partially disproportionated Co_2P phase within the amorphous carbon matrix acted as an inactive conductor and contributed to the fast rate capability.

Conclusions

The electrochemical reaction mechanism of conversion/partial recombination during discharge/charge for the CoP electrode was demonstrated utilizing ex situ XRD and EXAFS analyses on the basis of the DCP. Further modification of this system with carbon to form the CoP/C nanocomposite resulted in partial disproportionation of CoP in the nanocomposite. The nanocomposite consisted of well-dispersed CoP (active with Li) and Co_2P (inactive with Li) nanocrystallites, as well as amorphous P (active with Li) within the amorphous carbon matrix. When tested as an anode material for rechargeable Li-ion batteries, the partially disproportionated CoP/C nanocomposite electrode exhibited good electrochemical performance, including a high initial charge capacity of 531 mA h g^{-1} (or 855 mA h cm^{-3}), a cycling durability of 407 mA h g^{-1} (or 655 mA h cm^{-3}) over 200 cycles, a good initial coulombic efficiency of ca. 75%, and a fast rate capability (2C: 435 mA h g^{-1} and 3C: 410 mA h g^{-1}). These good electrochemical properties were attributed to the alleviation of the volume change by the uniform distribution of active CoP nanocrystallites, the prevention of active material agglomeration during cycling by the presence of well-dispersed inactive Co_2P nanocrystallites, the presence of the amorphous carbon matrix to buffer the volume expansion of the active materials, and the electrochemically driven partial recombination reaction during repeated discharge/charge reactions. The superior electrochemical performance of the CoP/C nanocomposite electrode makes it a promising potential anode material for Li-ion batteries.

Acknowledgements

This research was supported by the MSIP (Ministry of Science, ICT and Future Planning), Korea, under the "Creative ICT Convergence Human Resource Development" support program (NIPA-2014-H7501-14-1002) supervised by the NIPA (National IT Industry Promotion Agency).

Notes and references

[a]School of Materials Science and Engineering, Kumoh National Institute of Technology, Gumi, Gyeongbuk 730-701, Republic of Korea. E-mail: cmpark@kumoh.ac.kr; Fax: +82-54-478-7769; Tel: +82-54-478-7746
[b]School of Advanced Materials Engineering, Kookmin University, Seoul 136-702, Republic of Korea
[c]Department of Environmental Engineering, Inha University, 100 Inha-ro, Nam-gu, Incheon 402-751, Republic of Korea
[d]Outstanding Research Group Program, Convergence Technology Research Institute, Kumoh National Institute of Technology, Gumi, Gyeongbuk 730-701, Republic of Korea

†Footnotes should appear here. These might include comments relevant to but not central to the matter under discussion, limited experimental and spectral data, and crystallographic data.
Electronic Supplementary Information (ESI) available: [details of any supplementary information available should be included here]. See DOI: 10.1039/b000000x/

1. G.-A. Nazri and G. Pistoia, lithium batteries; science and technology, Kluwer academic/Plenum, Boston, 2004.
2. C.-M. Park, J.-H. Kim, H. Kim and H.-J. Sohn, *Chem. Soc. Rev.*, 2010, **39**, 3115.
3. M. Winter, J. O. Besenhard, M. E. Spahr and P. Novak, *Adv. Mater.*, 1998, **10**, 725.
4. R. A. Huggins, *J. Power Sources*, 1999, 81-82, 13.
5. R. Marom, S. F. Amalraj, N. Leifer, D. Jacob and D. Aurbach, *J. Mater. Chem.*, 2011, **21**, 9938.

6. P. G. Bruce, B. Scrosati and J.-M. Tarascon, *Angew. Chem., Int. Ed.*, 2008, **47**, 2930.
7. J. Cabana, L. Monconduit, D. Larcher and M. R. Palacin, *Adv. Energy Mater.*, 2010, **22**, E170.
8. H. Kim, G. Jeong, Y.-U. Kim, J.-H. Kim, C.-M. Park and H.-J. Sohn, *Chem. Soc. Rev.*, 2013, **42**, 9011.
9. N.-S. Choi, Z. Chen, S. A. Freunberger, X. Ji, Y.-K. Sun, K. Amine, G. Yushin, L. F. Nazar, J. Cho and P. G. Bruce, *Angew. Chem. Int. Ed.*, 2012, **51**, 9994.
10. D. Larcher, S. Beattie, M. Morcrette, K. Edstrom, J.-C. Jumas and J.-M. Tarascon, *J. Mater. Chem.*, 2007, **17**, 3759.
11. Y. Idota, T. Kubota, A. Matsufuji, Y. Maekawa and T. Miyasaka, *Science*, 1997, **276**, 1395.
12. Y.-C. Ha, C. Cho, Y.-U. Kim, C.-M. Park and H.-J. Sohn, *J. Korean Phys. Soc.*, 2011, **59**, 3458.
13. Y. Yamada, Y. Iriyama, T. Abe and Z. Ogumi, *J. Electrochem. Soc.*, 2010, **157**, A26.
14. H. Yamauchi, G. Park, T. Nagakane, T. Honma, T. Komatsu, T. Sakai and A. Sakamoto, *J. Electrochem. Soc.*, 2013, **160**, A1725.
15. G. R. Goward, L. F. Nazar and W. P. Power, *J. Mater. Chem.*, 2000, **10**, 1241.
16. M. Yoshio, T. Tsumura and N. Dimov, *J. Power Sources*, 2005, **146**, 10.
17. X. Feng, J. Yang, P. Gao, J. Wang and Y. Nuli, *RSC adv.*, 2012, **2**, 5701.
18. C. Du, C. Gao, G. Yin, M. Chen and L. Wang, *Energy Environ. Sci.*, 2011, **4**, 1037
19. C. K. Chan, H. Peng, G. Liu, K. McIlwrath, X. F. Zhang, R. A. Huggins and Yi Cui, *Nature Nanotech.*, 2008, **3**, 31.
20. S. Yoon, C.-M. Park, H. Kim and H.-J. Sohn, *J. Power Sources*, 2007, **167**, 520.
21. D. Deng, M. G. Kim, J. Y. Lee and J. Cho, *Energy Environ. Sci.*, 2009, **2**, 818.
22. Y. S. Jung, S. Lee, D. Ahn, A. C. Dillon and S.-H. Lee, *J. Power Sources*, 2009, **188**, 286.
23. K. M. Abraham, D. M. Pasquariello and E. B. Willstaedt, *J. Electrochem. Soc.*, 1990, **137**, A743.
24. P. Balaya, H. L. Kienle and J. Maier, *Adv. Funct. Mater.*, 2003, **13**, 621.
25. C.-M. Park and H.-J. Sohn, *Adv. Mater.*, 2007, **19**, 2465.
26. D. C. S. Souza, V. Pralong, A. J. Jacobson and L. F. Nazar, *Science*, 2002, **296**, 2012.
27. C.-M. Park, Y.-U. Kim and H.-J. Sohn, *Chem. Mater.*, 2009, **21**, 5566.
28. S. Boyanov, J. Bernardi, F. Gillot, L. Dupont, M. Womes, J.-M. Tarascon, L. Monconduit, and M.-L. Doublet, *Chem. Mater.*, 2006, **18**, 3531
29. J. Fullenwarth, A. Darwiche, A. Soares, B. Donnadieuc and L. Monconduit, *J. Mater. Chem. A.*, 2014, **2**, 2050.
30. C.-M. Park and H.-J. Sohn, *Chem. Mater.*, 2008, **20**, 6329.
31. H. Hwang, M. G. Kim, Y. S. Kim, W. Martin and J. Cho, *J. Mater. Chem.*, 2007, **17**, 3161.
32. K. Wang, J. Yang, J. Xie, B. Wang and Z. Wen, *Electrochem. Commun.*, 2003, **5**, 480.
33. M. C. L´opez, G. F. Ortiz and J. L. Tirado, *J. Electrochem. Soc.*, 2012, **159**, A1253.
34. Z. Zhang, J. Yang, Y. Nuli, B. Wang and J. Xu, *Solid State Ionics*, 2005, **176**, 693.
35. R. Alca´ntara, J.L. Tirado, J.C. Jumas, L. Monconduit and J. Olivier-Fourcade, *J. Power Sources*, 2002, **109**, 308.
36. Y.-H. Cui, M.-Z. Xue, Z.-W. Fu, X.-L. Wang and X.-J. Liu, *J. Alloys Comp.*, 2013, **555**, 283.
37. R. Khatib, A.-L. Dalverny, M. Saubanère, M. Gaberscek and M.-L. Doublet, *J. Phys. Chem. C*, 2013, **117**, 837.
38. V. Pralong, D.C.S. Souza, K.T. Leung and L.F. Nazar, *Electrochem. Commun.*, 2002, **4**, 516.
39. D. Yang, J. Zhu, X. Rui, H. Tan, R. Cai, H. E. Hoster, D. Y. W. Yu, H. H. Hng and Q. Yan, *ACS Appl. Mater. Interfaces*, 2013, **5**, 1093.
40. C.-M. Park and H.-J. Sohn, *Adv. Mater.*, 2010, **22**, 47.
41. C.-M. Park, S. Yoon, S.-I. Lee, J.-H. Kim, J.-H. Jung and H.-J. Sohn, *J. Electrochem. Soc.*, 2007, **154**, A917.
42. C.-M. Park and H.-J. Sohn, *Chem. Mater.*, 2008, **20**, 3169.
43. C.-M. Park and H.-J. Sohn, *Electrochim. Acta*, 2010, **55**, 4987.
44. C.-M. Park and H.-J. Sohn, *Electrochim. Acta*, 2009, **54**, 6367.
45. K. Ishida and T. Nishizawa, *Bull. Apd.*, 1990, **11**, 555.
46. P. Poizot, S. Laruelle, S. Grugeon, L. Dupont and J.-M. Tarascon, *Nature*, 2000, **407**, 496.
47. M. Wachtler, M. Winter and J. O. Besenhard, *J. Power Sources*, 2002, **105**, 151.
48. H. Li, Q. Wang, L. Shi, L. Chem and X. Huang, *Chem. Mater.*, 2002, **14**, 103.
49. S. Arico, P. Bruce, B. Scrosati, J.-M. Tarascon and W. V. Schalkwijk, *Nat. Mater.*, 2005, **4**, 366.
50. Suryanarayana, *Prog. Mater. Sci.*, 2001, **46**, 1.
51. C.-M. Park, W. Choi, Y. Hwa, J.-H. Kim, G. Jeong and H.-J. Sohn, *J. Mater. Chem.*, 2010, **20**, 4854.
52. M.-G. Park, J. H. Song, J.-S. Sohn, C. K. Lee and Cheol-Min Park, *J. Mater. Chem. A*, 2014, **2**, 11391.

